OPEN ACCESS

1st International Electronic Conference on Remote Sensing
22 June - 5 July 2015

Conference Proceedings Paper – Remote Sensing

Narrowband and Wideband Channel Sounding of an Antarctica to Spain Ionospheric Radio Link

Marcos Hervás[1,*], Rosa Ma Alsina-Pagès[1], Ferran Orga[1], Joan Lluís Pijoan[1] , David Badia[1] and David Altadill[2]

[1] GR-SETAD La Salle, Universitat Ramon Llull, Quatre Camins 30, 08022 Barcelona, Spain; E-Mails: ralsina@salleurl.edu (R.M.A.-P.); forga@salleurl.edu (F.O.); joanp@salleurl.edu (J.L.P.); david@salleurl.edu (D.B);

[2] Observatori de l'Ebre, (OE), CSIC - Universitat Ramon Llull, Horta Alta 38, 43520 Roquetes, Spain; E-Mail: daltadill@obsebre.es (D.A.);

***** Author to whom correspondence should be addressed; E-Mail: mhervas@salleurl.edu (M.H.); Tel.: +34-932902445; Fax: +34-932902385.

Published: 22 June 2015

Abstract: La Salle and Ebro Observatory have been involved in several joint projects about remote sensing in Antarctica for the last 11 years (approximately one solar cycle). The Ebro Observatory has been monitoring and analyzing the geomagnetic and the ionospheric activity in the Antarctic Spanish station Juan Carlos I, ASJI, (62.7ºS, 299.6 ºE) for more than eighteen and ten years respectively. La Salle has two main goals in the project. The first one is the data transmission and reception from Antarctica to Spain to obtain a historical series of measurements of channel sounding of this 12760 km ionospheric HF radio link. The second one is the establishment of a stable data low power communication system between the ASJI and Cambrils, Spain, (41.0ºN, 1.0ºE) to transmit the data from the remote sensors located in the island. In this paper, both narrowband and wideband soundings have been carried out to determine channel availability performed using a frequency range from 2 to 30 MHz with 0.5 MHz step during the 24 hours of the day, encompassing wider channel measurements than previously done, in terms of hours and frequency. This paper presents the results obtained for the austral summer in 2014, using a monopole antenna at the transmitter and an inverted V on the receiver side.

Keywords: geomagnetism; remote sensors; HF; ionosphere; channel sounding; Antarctica

1. Introduction

Analyzing the ionosphere and the magnetic field in the Antarctica is an important contribution to understand of Earth's phenomenons concerning the geophysical science. Knowledge acquired on the characteristics of the channel does not only improve the performance of high frequency (HF) radio-communication systems, but also develops ionospheric science. Vertical and oblique sounding techniques are frequently used to obtain the characteristics of the ionospheric channel for a given radio-link. The geomagnetic observatories have been collecting for years the magnetic field variations in fixed locations having a wide range of time scales, from seconds to centuries, to make possible the understanding of the behavior of the magnetic field of the Earth.

The Antarctic Spanish Station Juan Carlos I (ASJI) is located in the Livingston Island, a place of great interest because it monitors the sub-auroral zone [1]. The ASJI has a geomagnetic observatory with the International Association of Geomagnetism and Aeronomy code LIV. LIV is remotely managed by the Ebro Observatory Institute (EO) in Spain and it is aimed to monitor the magnetic field variations of that region. ASJI is only attended by scientist and technicians during the austral summer, typically from December to February. As ionospheric exploration by vertical soundings is one of the most commonly used to observe the vertical structure of the ionosphere, a VIS (Vertical Incidence Sounder) was installed at the ASJI during the summer expedition of 2004–2005 by OE. In 2003, an OIS (Oblique Incidence Sounder) was also installed in the ASJI by La Salle with a double objective: *i)* to measure the characteristics of the ionospheric channel from ASJI to Spain, taking into account days, annual and solar cycle variations and *ii)* to settle a robust hardware and software platform for an HF radio-communication system from ASJI to Spain. The later system should be able to operate under hard environmental conditions, with the best digital modulations designed for a low power and high interference communications system. The OIS covers a long haul ionospheric link (see Figure 1), of around 12760 km, from the ASJI (62.7ºS, 299.6 ºE) to Cambrils (41.0ºN, 1.0ºE).

In previous works, both narrowband and wideband soundings had been analyzed [2], but both carrier frequencies and the time of transmission were limited. Since 2008, an enhanced transmitter and receiver were installed [3], and the oblique sounding observations can be widely recorded. The results presented in this paper give light to the knowledge of this long haul link, but also help us to design the physical layer characteristics remaining from the previous studies [4,5], where less carrier frequencies were used and the tests were not performed during the entire day.

Figure 1. Geographical link characteristics. The transmitter is located in the ASJI, in Livingston Island (62.7ºS, 299.6 ºE) and the receiver is placed in Cambrils (41.0ºN, 1.0ºE).

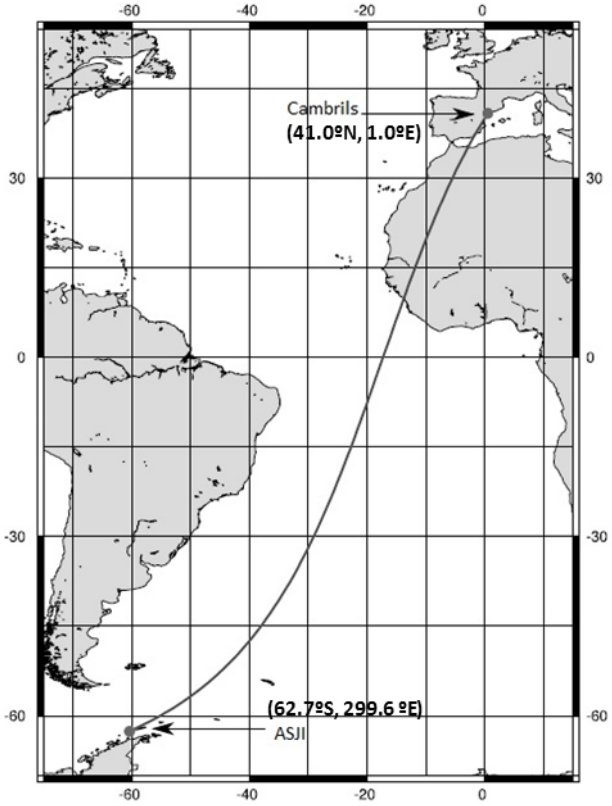

This paper is organized as follows. Section 2 describes all the measured parameters. Section 3 gives details of the communications hardware equipment between the Remote Geophysical Observatory and Spain. Section 4 explains the test design for narrowband and wideband sounding measurements through a long-distance HF link in 2014 campaign. Section 5 presents the results of the sounding measurements. Finally, section 6 contains the conclusions and the future work.

2. Measured Parameters

This section describes the main sensors located at the ASJI and its measurements.

2.1. Measurements of Geomagnetic Parameters

Measuring geomagnetic parameters is a complex task due to the fact that the physical magnitude to be measured is a vector. This requires an accurate determination of the magnitudes with respect to a fixed reference frame and skilled staff from both technical and scientific point of view.

The geomagnetic vector can be given in either three of coordinate systems based on a geographic reference: *i)* Cartesian: where X, Y, Z are the geographic north, east and altitude projections respectively. *ii)* Cylindrical: where H and Z are the horizontal and altitude projections and D is the declination angle between the geographic north and the magnetic field, establishing that the positive is towards east. *iii)* Spherical: where F is the total vector magnitude, D is the declination and I is the

inclination angle between the horizontal projection and the magnetic vector itself, establishing positive downwards.

As far as the geomagnetic sensors are concerned, a D/I fluxgate theodolite (see Figure 2) is mounted in the first hut of the ASJI. This sensor permits a manual measurement of the Declination and Inclination angles of the vector magnetic field in absolute terms, which permits to discuss about the uncertainties of this instrument [6]. It consists of a fluxgate magnetometer bar mounted on the telescope of a non-magnetic theodolite.

Figure 2. The manual D/I fluxgate theodolite being manipulated by a specialist.

A variometer type δD/δI vector magnetometer (see Figure 3) is mounted in the second hut to measure automatically the variations of the magnetic field vector once per minute. It consists of two perpendicular pairs of Helmholtz coils the polarization of which allows measuring the Declination and Inclination variations with a Proton magnetometer located at their center [7]. The Proton magnetometer measures the total magnetic field intensity, F, when the coils are not polarized.

Figure 3. The δD/δI vector magnetometer deployed at the ASJI with the two perpendicular pairs of Helmoltz coils and the Proton magnetometer allowing to measure the variations of D and I.

The last of these three huts houses the electronic system controlling this automatic instrument. A new three-axis fluxgate magnetometer (see Figure 6) was added during the 2008 expedition. It is able to measure automatically the magnetic field variations from an analogue output sampling at both 1 and 0.1 Hz by the corresponding Analog to Digital Converter, ADC.

Figure 4. The three-axis automatic fluxgate magnetometer was added in 2008.

Once the raw data is processed, the definitive data set is sent to the World Data Centers becoming accessible to the scientific community. Nowadays, a real-time access to the data is provided through a satellite link thanks to the International Real-time Magnetic observatory (INTERMAGNET). Nevertheless, a reliable skywave link designed by La Salle and the Ebro Observatory is active as a backup. A future project is motivated to separate our sensor data from the INTERMAGNET link and transmit only through the autonomous skywave link which, besides, is becoming another interesting sensor of the ionosphere due to the capability of measuring the ionosphere performance.

2.2. Vertical incidence soundings of the ionosphere

A Vertical Incidence ionospheric Sounder (VIS) was installed at the ASJI (Figure 5) during the 2004-2005 survey to provide information of the ionospheric characteristics in this region. Data provided by the VIS is used to characterize the climatology of the ionosphere and to investigate the ionospheric effects caused under geomagnetically disturbed periods.

Figure 5. The VIS installed at the ASJI is the Advanced Ionospheric Sounder (AIS) developed by the *Instituto Nazionale di Geofisica e Vulcanologia* (INGV) of Rome, Italy. For more details about the ionosonde see [8].

The VIS located at the ASJI records a vertical incidence ionogram every 10 minutes. A ionogram is a graph that represents the time-of-flight for every radio frequency transmitted vertically and received after its reflection in the ionosphere. Figure 6 shows an example of a ionogram recorded by the VIS at the ASJI where the particular layers of the ionosphere can be seen clearly. For more details about the VIS soundings see [9].

Figure 6. An example of a ionogram recorded by the VIS at the ASJI where one can see clearly the particular layers of the ionosphere.

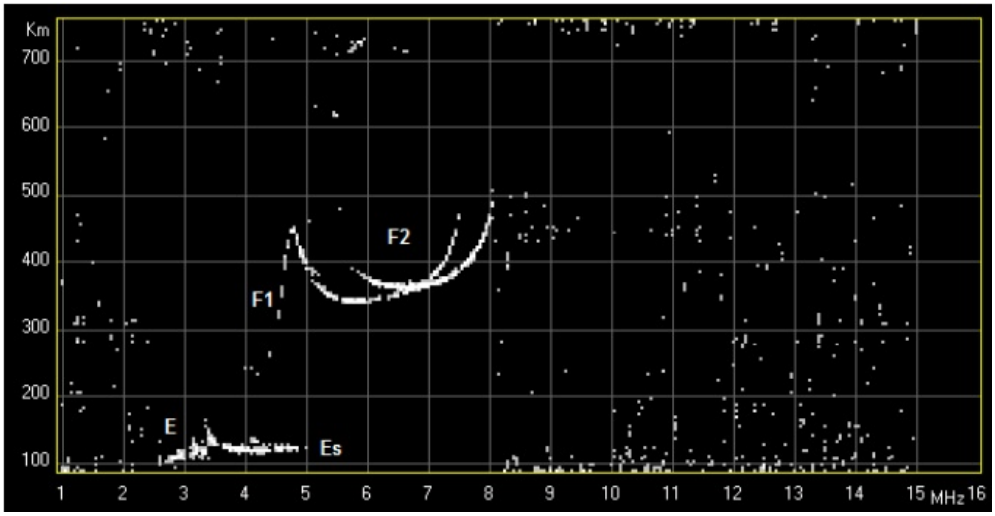

2.3. Oblique incidence soundings of the ionosphere

The oblique ionosonde is developed by La Salle to analyze and characterize the ionospheric channel between Antarctica and Spain [2]. It is used to obtain useful and key parameters for modeling the HF radio link; i.e, link availability, power delay profile of the channel and frequency dispersion. The soundings are carried out during the austral summer, when the ASJI is operative, the transmitter antenna is located at the ASJI (see Figure 7), and the receiver is located in Cambrils, Spain. More details of the HF data transmission are given in the section 4.

Figure 7. The antenna of the oblique ionosonde transmitter in the ASJI.

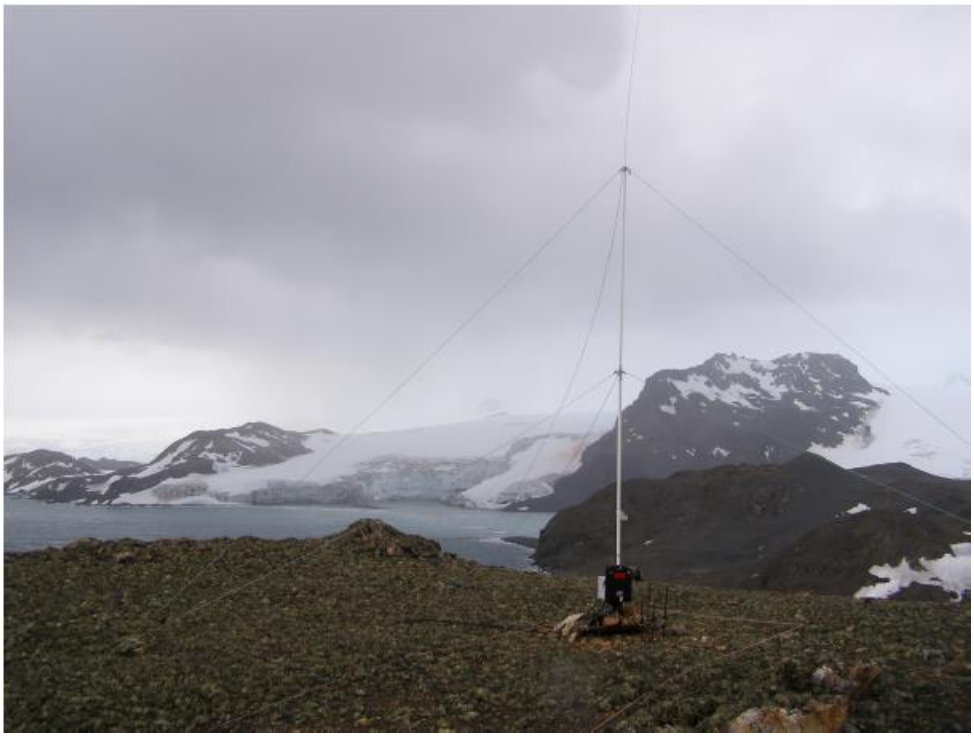

3. System Description

The hardware of the ionospheric channel sounder jointly with the oblique ionosonde and data transmission system has been designed in order to have an extended frequency range and to get the best frequency and time accuracy. Moreover, the whole transmission system has been entirely redesigned compared to the initial system deployed on the survey 2003-2004 [2]. It was upgraded with faster and more reliable equipment during the 2009-2010 expedition. As a result of the last improvement, the system is able to operate at a higher bandwidth up to 40 KHz and to sample at 100 ksps. Also the system was redesigned to be more flexible concerning the frequency and bandwidth selection for the soundings.

The main features of the transmitter and receiver hardware are described below.

3.1. Hardware of the Transmitter

The core is composed by an embedded PC with a Digital Signal Processing (DSP) unit inside which performs the tasks of controlling and configuring the system parameters. The main DSP unit is the XTremeDSP-IV from Nallatech and it includes 3 Xilinx FPGA[1] described below: *i)* a Virtex-II is responsible for clock configuration, *ii)* a Spartan-II handles the interface between the PCI bus and *iii)* a Virtex-4 which performs the software radio procedures. In order to perform these software radio operations, the Virtex-4 is equipped with two 14-bit ADC, two 14-bit DAC and all the arithmetic and peripheral drivers. Figure 8 shows a block diagram of the transmitter.

Figure 8. Scheme of the transmitter that consists of an embedded digital platform and different peripherals used to control the system and to improve the synchronization.

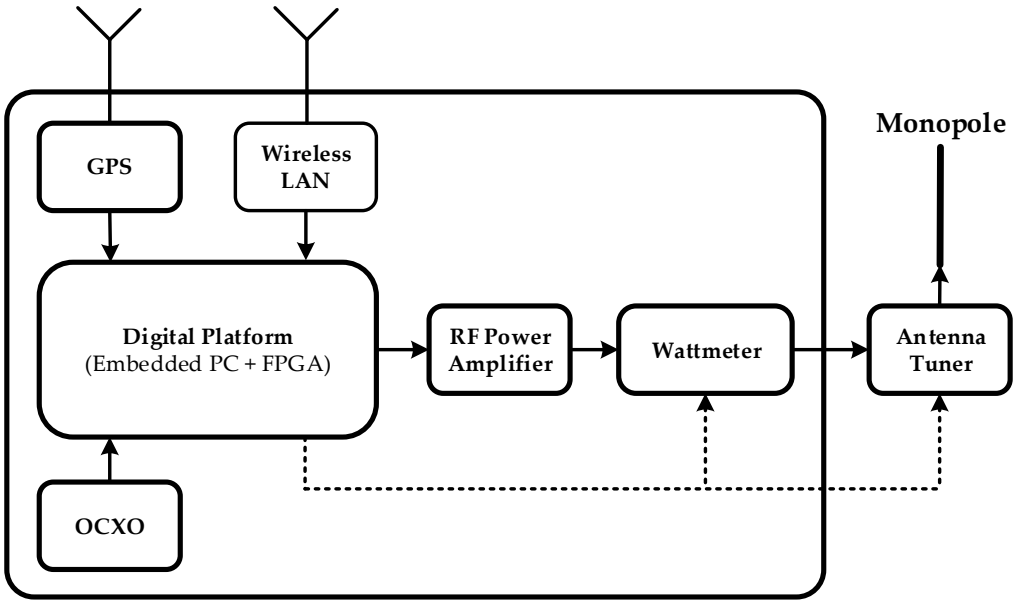

[1] FPGA stands for Field Programmable Gate Array, and it is an integrated circuit to be configured after manufacturing.

Moreover, a GPS unit is placed to make possible the time synchronization using the Pulse Per Second (PPS) signal, which makes possible to measure the propagation time of the wave with an accuracy of 1 μs. Also, a 100 MHz Oven Controlled Crystal Oscillator (OCXO) is installed in both transmitter and receiver in order to increase the frequency synchronization accuracy. The Wattmeter measures the forward and reverse transmitted power in order to notice severe impedance mismatch. And the FPGA is capable, thanks to its peripheral drivers, to switch off the amplifier in case of malfunctioning. The Antenna Tuner is used to tune semi-automatically the monopole antenna, which transmits the signal.

As far as the deployment is concerned, all the transmitter hardware is close to the antenna at the top of a hill near to the ASJI. All the electronics is sealed inside a watertight box which protects against severe weather conditions and provides electromagnetic shielding. The system is remotely accessed through a Wireless Local Area Network (WLAN) from the laboratory in the ASJI.

3.2. Hardware of the Receiver

An inverted-V antenna is used to get the signal in the receiver. As shown in Figure 9, the radio frequency signal is passed through a certain filtering and amplification process, and given next to the digital platform, which works the same way as the transmitter described above.

Moreover, the receiver also has an OCXO and a GPS to improve both frequency and time synchronization. A block diagram of the receiver is shown in Figure 9.

Figure 9. Scheme of the receiver that consists of several filtering stages and a digital platform with peripherals to improve synchronization.

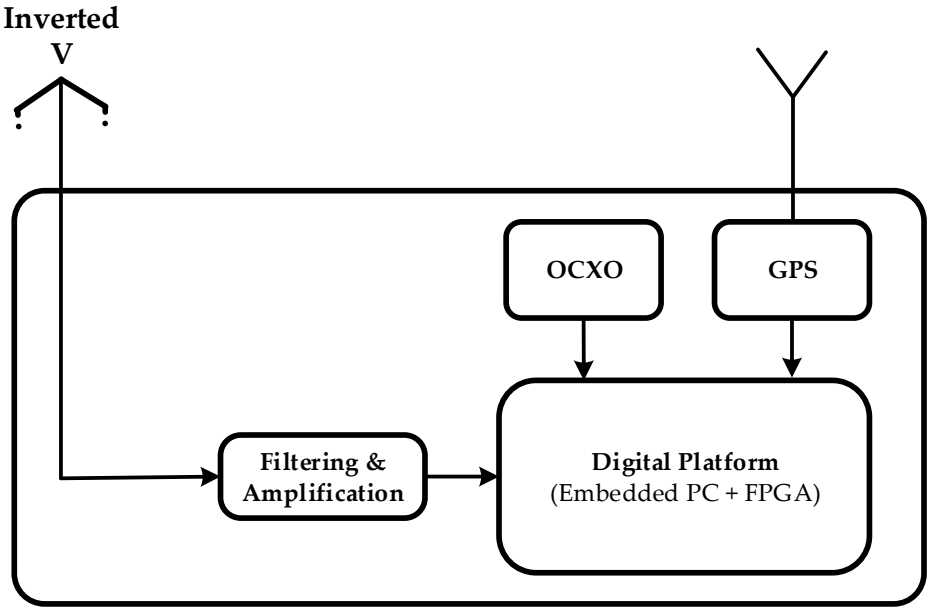

4. Data analysis

This section presents a detailed explanation of the test description and the analysis algorithms for narrowband and wideband oblique sounding.

4.1. Tests Description

The analysis of the sounding channel has been carried out in both narrowband and wideband. While the narrowband analysis focuses on channel availability and Signal to Noise Ratio (SNR), the wideband calculates the scattering function from the estimated channel impulse response, and then evaluates the multipath delay spread and Doppler spread.

The soundings are carried out during 24 hours a day (sessions) for a frequency carrier ranging from 2 to 30 MHz with steps of 500 Hz which corresponds to 57 sub-sessions. Every sub-session is divided into a frame to subdivide the time into two experiments, using 40 s for both of them. Finally, every session has a time slot of 22 minutes (called ‘others’ in the figure) to transmit the data from the sensors, and to test also new modulations schemes. The structure of the periodic experiment conducted during the 2013-2014 campaign can is described in Figure 10. These soundings were carried out for 25 days, between January 25th and February 18th.

The idle intervals are included in all frames to ensure the system to guarantee synchronization. The antenna tuning of 20W is required because the transmitter antenna is a monopole. The channel sounding is carried out in the processes called ‘tone’ and ‘PseudoNoise (PN) sequence’ during 10 s each.

Figure 10. Frame structure of the channel sounding.

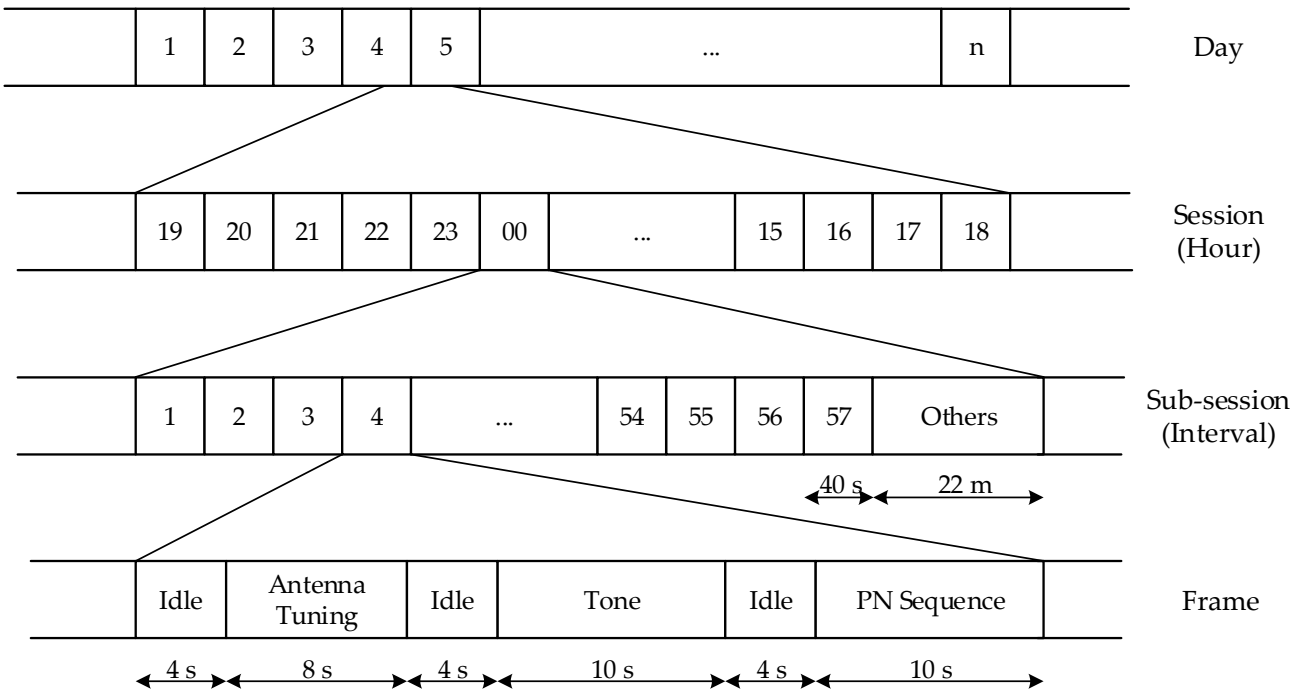

The narrowband analysis is necessary to characterize the channel in terms of SNR and availability, using a sine wave as the transmitted signal. This tone is transmitted during 10 s. The configuration parameters are detailed in Table 1.

Table 1. Configuration parameters and setup for the narrowband sounding in 2013-2014 survey.

Parameter	Value
Signal	Sine wave
Duration	10 s
Silence	4 s

The wideband analysis is necessary to characterize time and frequency dispersion in the channel. The transmitted signal for the wideband analysis is a PN sequence [10] with the configuration parameters detailed in Table 2.

Table 2. Configuration parameters and setup for the wideband sounding in 2013-2014 survey.

Parameter	Value
Sampling frequency	100 kHz
PN sequence length	127
Family of sequences	m-sequence
Chip frequency	5 kHz
Number of sequences per test	300

4.2. Narrowband Analysis

The narrowband analysis focuses on SNR and channel availability computation. The channel availability is defined as the probability of a link to reach a minimum SNR value and therefore achieving a certain quality of service (see [11] for more details). A minimum SNR value of 6 dB was specified to estimate the channel availability in a bandwidth of 10 Hz [2]. In order to improve the reliability of the detection system, due to the probability of high noise and interference, several techniques were developed in [3]. SNR is computed with the comparison between the received power measured during the tone intervals and the noise power measured during the idle periods.

The first step is to filter the signal to obtain a usable power profile, conducted in frequency domain with the Fast Fourier Transform (FFT). Afterwards, a windowing is applied to *i)* remove the non-desirable signals out of the reception frequency and *ii)* avoid creating transients from the impulsive interferences falling far away from the reception frequency [3] when an ideal filter is used. Previous tests showed that the Kaiser window presents a better smooth response [3].

The measurements of SNR can be distorted easily because of high level of interferences. To overcome this problem a time framing technique is used, consisting on dividing the tone interval in 10 smallest sub-intervals of 1 s each, and observing the evolution of the SNR along the whole interval (see in Figure 11).

Figure 11. Diagram of time framing technique for narrowband sounding.

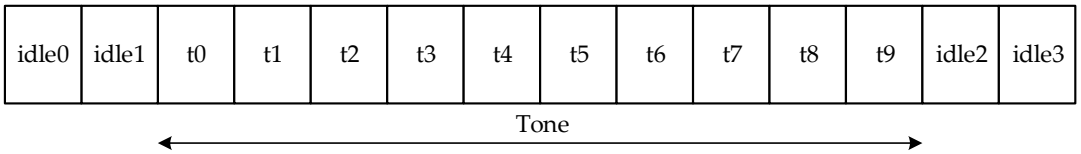

According to previous experiments, two SNR threshold values are defined, $Th_{Low} = 3dB$ and $Th_{HIGH} = 6dB$. Only those measurements that fulfill $SNR \geq Th_{Low}$ over 70% of the segments or $SNR \geq Th_{HIGH}$ over 50% of the segments are taken into account to estimate the SNR and channel availability. An estimation of the SNR result of February 17th is shown in Figure 12.

Figure 12. SNR of February 17th (in dB) over a bandwidth of 10 Hz, in which the regions of day, night, sunrise and sunset can be appreciated

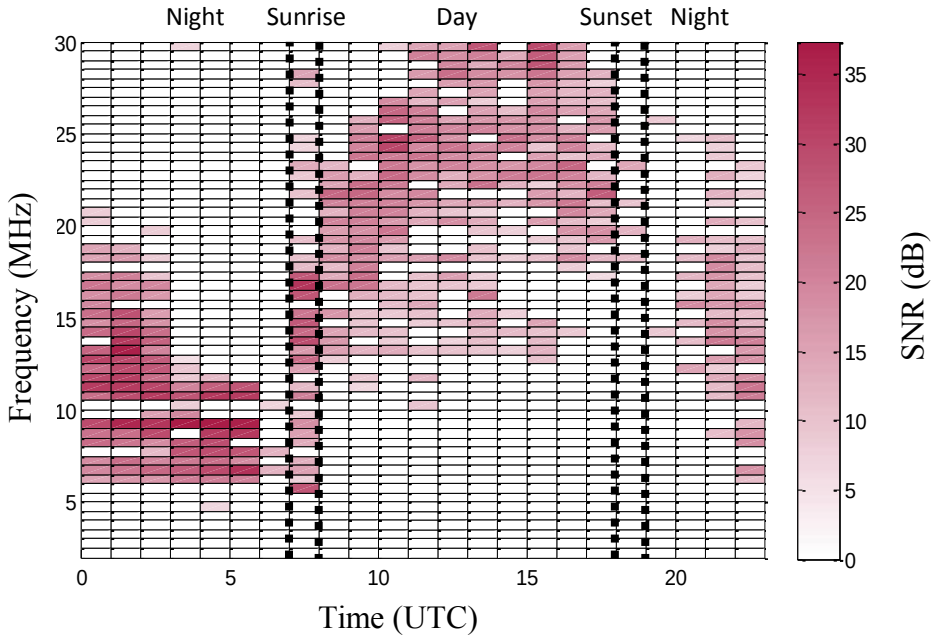

4.3. Wideband Analysis

The wideband analysis is performed sending PN waveforms with good cyclic cross-correlation characteristics, therefore using M-sequences [12]. The computation process for the wideband sounding is detailed in Figure 13.

Figure 13. Diagram of the computation process for wideband channel sounding.

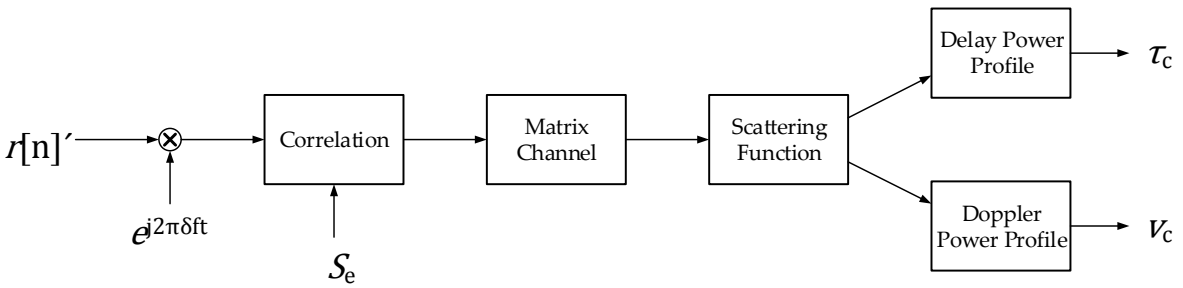

The wideband analysis is crucial to characterize time and frequency dispersion in the channel. First, the received signal *r[n]* (with the characteristics described in 4.1) is correlated with the original PN sequence S_e. The correlation function is calculated as

$$\phi_{r,S_e}[n] = \sum_{k=0}^{N_e-1} r[n+k]S_e[k] \quad (1)$$

where N_e is the length of the PN sequence. Hence, the channel impulse response $h[n,\tau]$ can be written as:

$$h[n,\tau] = \phi_{r,S_e}[nlN_c + \tau] \quad (2)$$

where τ is the delay variable, l is the number of chips and N_c is the number of samples per chip. From equation 2, the following parameters are calculated: scattering function, composite multipath spread and composite Doppler spread. The scattering function $R_s[\tau,\upsilon]$ is calculated as the FFT of the channel impulse response [12].

$$R_h[\xi,\tau] = \sum_{\xi} h^*[n,\tau]\, h[n+\xi,\tau] \quad (3)$$

$$R_s[\tau,\upsilon] = \sum_{\xi} R_h[\xi,\tau]e^{-j2\pi\xi\upsilon} \quad (4)$$

Both the composite multipath spread and the composite Doppler spread are calculated from the data obtained in the scattering function $R_s[\tau,\upsilon]$. Let $[\tau_1,\tau_2]$ be the multipath observation window, and $[\upsilon_1,\upsilon_2]$ the Doppler spread observation window. Consequently, both multipath power profile is defined as

$$\phi[\tau] = \sum_{\upsilon=\upsilon_1}^{\upsilon_2} R_s[\tau,\upsilon] \quad (5)$$

And the Doppler power profile is defined as

$$\phi[\upsilon] = \sum_{\tau=\tau_1}^{\tau_2} R_s[\tau,\upsilon] \quad (6)$$

In this work, the window have been set to [-3.5,3.5] (ms) and [-2.5,2.5] (Hz) respectively, due to maximum delay and Doppler spread values obtained in previous tests [2].

Next, the spread parameters are calculated. The multipath spread is measured from the multipath power profile as the 80% of the power spread [2]. This parameter is named composite multipath spread (t_{eff}) and was defined in [13]. The same way, the Doppler spread is measured from the Doppler power profile as the 80% power spread. It is named composite Doppler spread (u_{eff}), and it was defined in [14].

In Figure 14 we can observe the performance of the wideband sounding of the February 1st 2014, at 00 UTC for 13 MHz of carrier frequency. In Figure 14.a the channel response $h[n,\tau]$ is plot, and the channel variations along time can be observed. In Figure 14.b, the scattering function has been calculated using $h[n,\tau]$, and $R_s[\tau,\upsilon]$ is obtained after performing the FFT. In Figure 14.c, the

multipath power profile is observed for the previously defined time window, and finally, in Figure 14.e, the Doppler power profile is plotted for the previously defined frequency window.

Figure 14. Wideband channel response and measures for February 01st 2014 at 07 UTC with 13 MHz of carrier frequency: **(a)** normalized channel response $h[n,\tau]$, **(b)** normalized scattering function $R_s[\tau,\upsilon]$, **(c)** multipath power profile (in ms), **(d)** the integral of the multipath power profile to calculate delay spread (in ms), **(e)** Doppler power profile (in Hz), and **(f)** the integral of the Doppler power profile to calculate Doppler spread (in Hz).

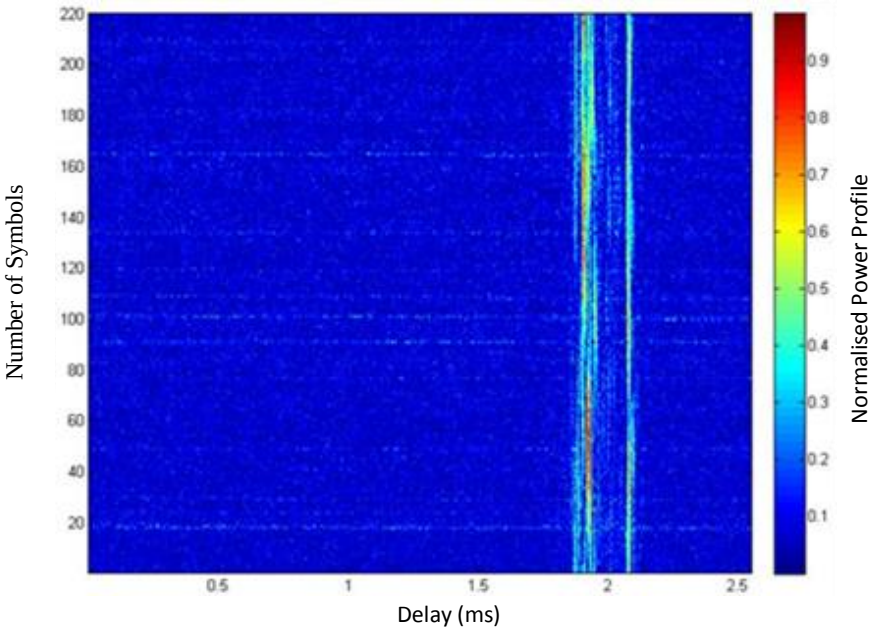

(a)

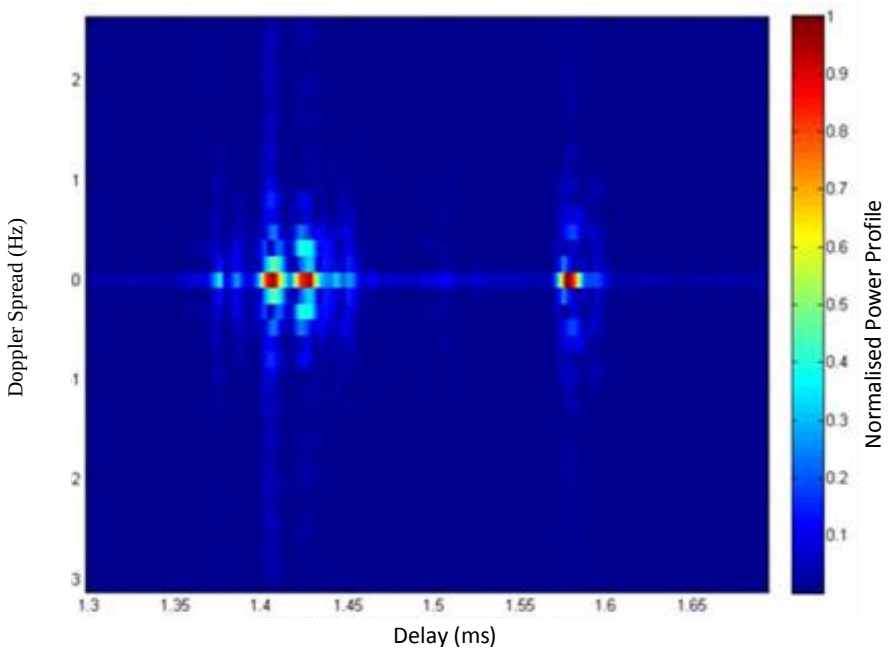

(b)

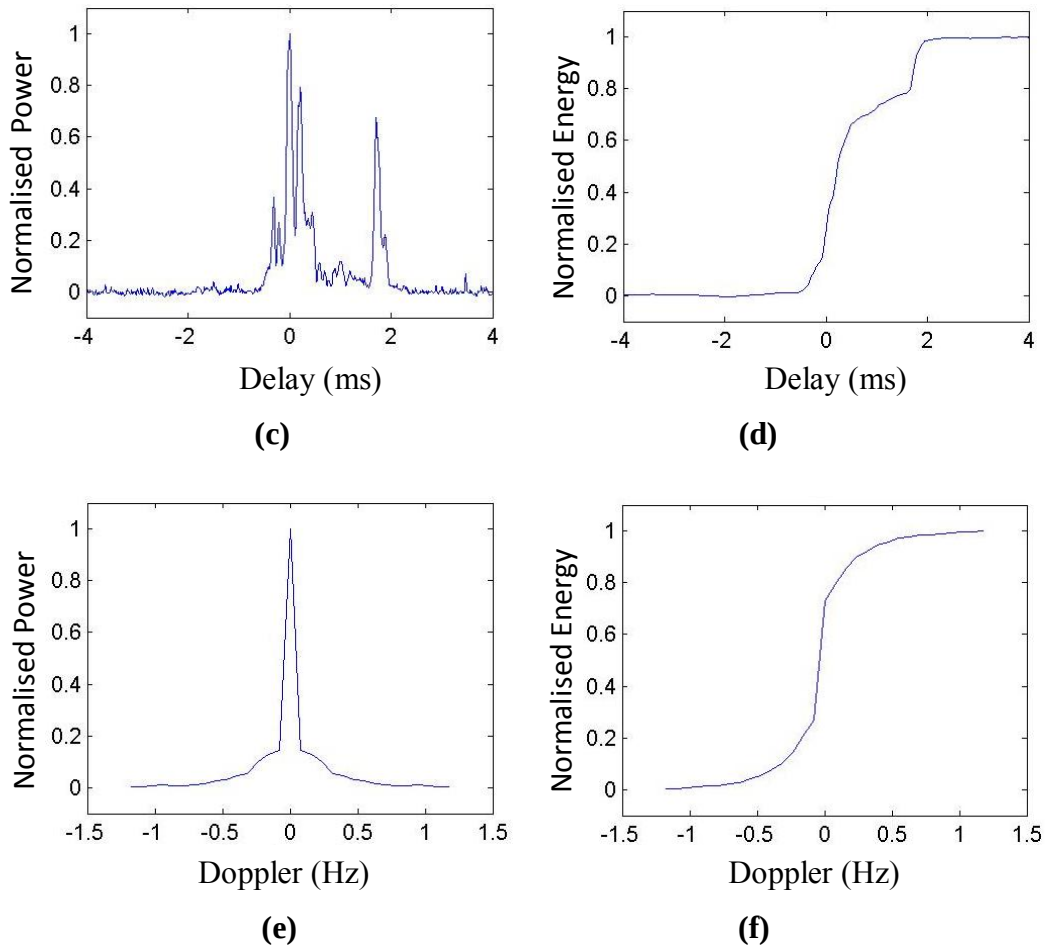

5. Results

5.1. Narrowband Results

The results of narrowband analysis shown in Figure 15 represent the average plot of the channel availability for the survey. Figure 15 depicts the channel availability for frequencies ranging from 2 to 30 MHz as function of time. The Frequency of Largest Availability (FLA) for a particular time is shown as dashed line. Four different zones can be distinguished: day, night, sunrise and sunset.

During the day interval, from 08 UTC to 17 UTC, the frequencies ranging from 20 to 30 MHz present the better performance in terms of SNR. For the sunset period, around 18 UTC, the interval of frequencies that performs best falls linearly with the time between 20 and 30 MHz to 10 and 20 MHz. The night period is defined from 19 UTC to 06 UTC and the frequencies ranging from 6 to 15 MHz show the best results. Finally, for the sunrise, which is the period defined around 07 UTC, its best operation frequencies increase linearly with the time from frequencies between 6 and 15 MHz to frequencies ranging from 20 to 30 MHz.

In consequence, we can conclude the best reflective frequencies during the daytime are the highest frequency range, the nighttime the lowest one, and sunrise and sunset are regions of switching between these periods of time performing in an unstable condition for all frequencies. It is worth noticing a drop in the FLA after sunrise (9-10 UT) and a post sunset jump (20-21 UT) of the FLA. These effects deviate from the expected smooth transition of the FLA from nighttime to daytime conditions and vice versa.

Figure 15. Channel availability of the campaign 2014 measured during the austral summer, from January 25th to February 18th.

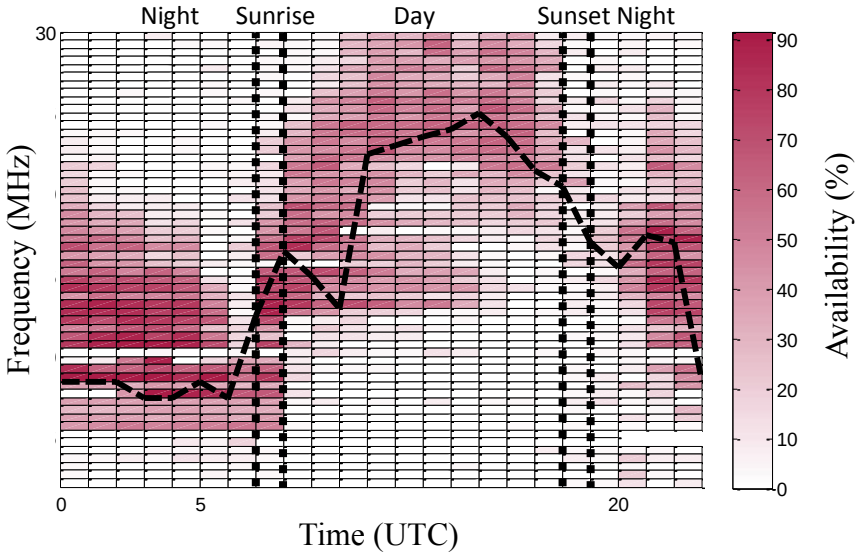

5.2. Wideband Results

The results of wideband analysis are shown in Figure 16. Figure 16.a and Figure 16.c, present the mean delay spread and the mean Doppler spread, from which one can distinguish four different performance zones also: day, night, sunrise and sunset [13]. Figure 16.b and Figure 16.d show the standard deviation for the delay spread and the Doppler spread respectively.

During day interval, from 08 UTC to 17 UTC, high frequencies ranging from 20 MHz to 30 MHz show the higher delay spread and Doppler spread of all measures. This means that the channel is available for a wide range of frequencies but its channel response is varying and unstable, and the intersymbol interference caused by a long channel response will be an important parameter for the modulation design.

Sunset time, around 18 UTC, presents an irregular performance when comparing high frequencies and low ones, but low frequencies start performing better while high frequencies decrease its availability. Also sunrise, around 07 UTC shows unstable performance in terms of wideband availability.

Nighttime, shown both on the right and on the left of Figure 16, ranging from 19 UTC to 06 UTC, present the best measurements in terms of channel availability and parameters. Best frequencies are around 10 MHz, despite channel is available until 20 MHz. Delay spread mean values are around 2 or 3 ms, with low deviation, and maximum Doppler spread values are around 0.7 Hz.

Figure 16. Mean value for the Delay Spread in ms **(a)**, standard deviation for Delay Spread in ms **(b)**, mean value for Doppler Spread in Hz **(c)** and standard deviation for Doppler Spread in Hz **(d)**.

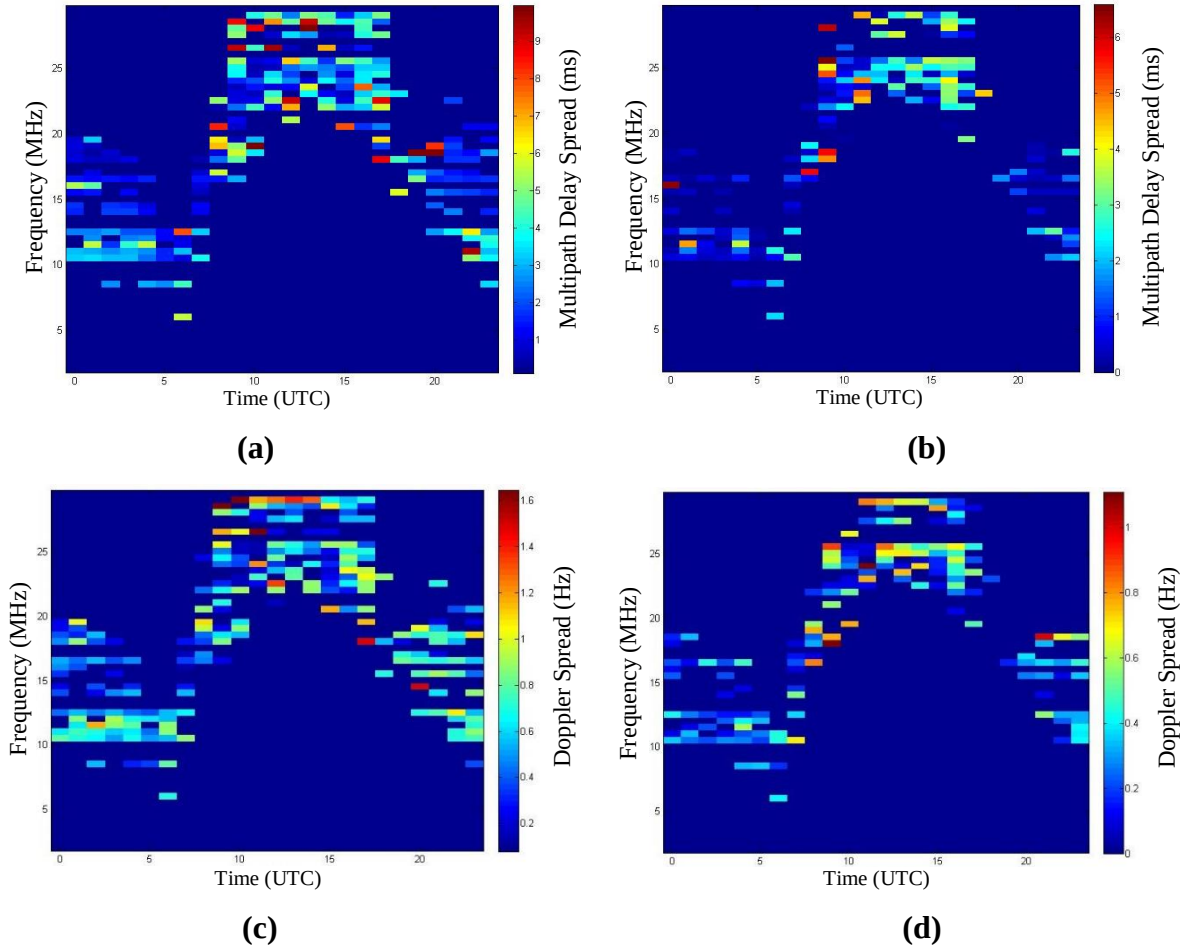

5.3. Discussion

Narrowband and wideband analysis conducted show similar results in terms of availability depending on the hour of the day. Nighttime is the best reception time, using frequencies from 8 MHz to 20 MHz. Narrowband presents its best SNR results while wideband shows its smaller delay spread and Doppler spread measurements.

These results allow us to conclude that for the best hours and frequencies, high throughput modulations like OFDM should be used, in order to increase the bit rate of the communication. Delay spread and Doppler spread won't worsen the results in a severe way, according to the measured values. Despite of that, the OFDM modulation should be designed taking into account coherence time and coherence bandwidth calculated using the measured parameters of Doppler spread and delay spread. Finally, at sunrise, sunset and daytime, a more robust modulation should be used. Direct sequence spread spectrum could be a good option assuming lower throughput, but assuring a more robust communication against channel variations or fadings.

6. Conclusions

This paper presents the main results of the oblique sounding measurement recorded during the campaign of 2014 with a transmitter placed in the Remote Geophysical Observatory of the ASJI and the receiver located in Cambrils (Spain). The sounding has been carried out for both narrowband and wideband to characterize the channel in terms of SNR, availability, multipath delay spread and Doppler spread. These measurements of the long haul link improve the knowledge of the performance of the ionospheric channel 12760 km long, and allow us to fully define the physical layer to send the data of the remote sensors deployed among the island from the Antarctica to Spain.

The values measured of narrowband and wideband confirm that both soundings show similar results in terms of availability depending on the hour of the day and of the frequency. Furthermore, the wideband analysis present results of the period of the day that is more suitable for data transmission, because the channel shows a good performance (with low Doppler spread and low delay spread). It also describes the hours of the day when the channel measurements, despite showing some availability, present worst results. This leads us to design a proper robust modulation for those hours, while the best transmission hours and frequencies use high throughput modulation techniques.

The future work is focused on two main goals. The first one is the study of the historical series of Doppler spread, delay spread and SNR for the entire solar cycle (around 11 years), using part of the data we have already measured. We are also working in including the number of paths in the receiver as a channel measurement in the wideband analysis. The second goal is to end the design of the HF modem; the channel characteristics shown in this paper are crucial for a proper design of the modulation, coding and interleaving of the physical layer of the modem.

Acknowledgments

This research has been supported by the Spanish Government under projects CTM2010-21312-C03-03 and –C03-01. In addition to the authors of this paper, the following people have been part of the research groups of these projects: Ahmed Ads, Raúl Bardají, Estefania Blanch, Oscar Cid, Juan José Curto, Simó Graells, Miguel Ibáñez, Joan Mauricio, Santiago Marsal, Joan Ramon Regué, Xavier Rosell, Martí Salvador, Antoni Segarra, José Germán Solé and Joan Miquel Torta.

Author Contributions

Marcos Hervás analyzed and wrote the part of the paper related with the narrowband soundings. Dr Rosa Ma Alsina-Pagès had the idea to write this paper, and analyzed and wrote the wideband sounding study in this paper. Ferran Orga wrote the introductory part, the measured parameters and the system description of this paper. Dr Joan Lluis Pijoan has been the principal investigator of project –C03-03, he has been involved in the part of channel sounding and testing of advanced modulations and reviewed the paper. Dr David Badia installed the transmission system in Antarctica, installed the receiver system in Spain and reviewed the paper. Dr David Altadill has been the principal investigator of project –C03-01 and coordinator of both projects and he has reviewed the paper.

Conflicts of Interest

The authors declare no conflict of interest.

References and Notes

1. Torta, J.M.; Gaya-Piqué, L.R.; Riddick, J.C.; Turbitt, C.W. A Partly manned geomagnetic observatory in Antarctica provides a reliable data set. *Contrib. Geophys. Geodesy Geophys. Inst. Slov. Acad. Sci.* **2001**, *31*, 225–230.
2. Vilella, C.; Miralles, D.; Pijoan, J.L. An Antarctica-to-Spain HF ionospheric radio link: Sounding results. *Radio Sci.* **2008**, doi:10.1029/2007RS003812.
3. Ads, A.G.; Bergadà, P.; Vilella, C.; Regué, J.R.; Pijoan, J.L.; Bardají, R.; Mauricio, J. A comprehensive sounding of the ionospheric HF radio link from Antarctica to Spain. *Radio Sci.* **2012**, doi:10.1029/2012RS005074.
4. Hervás, M.; Pijoan, J.L.; Alsina-Pagès, R.M.; Salvador, M.; Badia, D. Single-carrier frequency domain equalization proposal for very long haul HF radio links. *Electron. Lett.* **2014**, 17, 1252-1254, doi: 10.1049/el.2014.1184.
5. Bergadà, P.; Alsina-Pagès, R.M.; Pijoan J.L.; Salvador, M.; Regué, J.R.; Badia D.; Graells, S. Digital transmission techniques for a long haul HF link: DS-SS *vs.* OFDM. *Radio Sci.* **2014**, doi:10.1002/2013RS005203.
6. Marsal, S.; Torta, J.M. An evaluation of the uncertainty associated with the measurement of the geomagnetic field with a D/I fluxgate theodolite. *Measur. Sci. Technol.* **2007**, *18*, doi:10.1088/0957-0233/18/7/046.
7. Marsal, S.; Torta, J.M.; Riddick, J.C. An assessment of the BGS δDδI vector magnetometer. *Publs. Inst. Geophys. Pol. Acad. Sci.* **2007**, *99*, 158–165.
8. Zuccheretti, E.; Bianchi, C.; Sciacca, U.; Tutone, G.; Arokiasamy, J. The new AIS-INGV digital ionosonde. *Ann. Geophys.* **2003**, *46*, 647–659.
9. Bergadà, P.; Deumal, M.; Vilella, C.; Regué, J.R.; Altadill, D.; Marsal, S. Remote sensing and skywave digital communication from Antarctica. *Sensors* **2009**, doi:10.3390/s91210136.
10. Golomb, S. *Shift Register Sequences*; Holden-Day: San Francisco, USA, 1967.
11. Goodman, J.; Ballard, J.; Sharp E. A long-term investigation of the HF communication channel over middle- and high-latitudes paths. *Radio Sci.* **1997**, 32, 1705–1715, doi:10.1029/97RS01194.
12. Proakis, J. *Digital Communications*, 4th ed.; McGraw Hill: Boston, MA, USA, 2000.
13. Angling, M.J.; Davies N.C. An assessment of a new ionospheric channel model driven by measurements of multipath and Doppler spread. In Proceedings of the 1999 IEEE Colloquium on Frequency Selection and Management Techniques for HF Communications, London, UK, 29–30 March 1999.
14. Warrington, E.M.; Stocker A.J. Measurements of the Doppler and multipath spread of the HF signals received over a path oriented along the midlatitude trough. *Radio Sci.* **2003**, *38*, doi:10.1029/2002RS002815.

© 2015 by the authors; licensee MDPI, Basel, Switzerland. This article is an open access article distributed under the terms and conditions of the Creative Commons Attribution license (http://creativecommons.org/licenses/by/4.0/).